Riboswitch Tuning

DOI: 10.1002/ange.201407385

Tuning Riboswitch-Mediated Gene Regulation by Rational Control of Aptamer Ligand Binding Properties**

*Ambadas B. Rode, Tamaki Endoh, and Naoki Sugimoto**

Abstract: *Riboswitch-mediated control of gene expression depends on ligand binding properties (kinetics and affinity) of its aptamer domain. A detailed analysis of interior regions of the aptamer, which affect the ligand binding properties, is important for both understanding natural riboswitch functions and for enabling rational design of tuneable artificial riboswitches. Kinetic analyses of binding reaction between flavin mononucleotide (FMN) and several natural and mutant aptamer domains of FMN-specific riboswitches were performed. The strong dependence of the dissociation rate (52.6-fold) and affinity (100-fold) on the identities of base pairs in the aptamer stem suggested that the stem region, which is conserved in length but variable in base-pair composition and context, is the tuning region of the FMN-specific aptamer. Synthetic riboswitches were constructed based on the same aptamer domain by rationally modifying the tuning regions. The observed 9.31-fold difference in the half-maximal effective concentration (EC_{50}) corresponded to a 11.6-fold difference in the dissociation constant (K_D) of the aptamer domains and suggested that the gene expression can be controlled by rationally adjusting the tuning regions.*

Synthetic riboswitches have the potential to program cellular functions, sense bioactive molecules, and mediate antibacterial therapy.[1,2] Like their natural counterparts,[3] the functions of synthetic riboswitches are triggered in response to a specific target molecule. The aptamer domain that recognizes the specific ligand is indispensable for function of both natural and synthetic riboswitches. Synthetic riboswitches are generally constructed by linking an aptamer specifically selected from an RNA library with an expression platform; the function of the aptamer is to control gene expression from this platform.[1,2] Most synthetic riboswitches exhibit ON or OFF responses[2] in which the gene expression is either permitted or inhibited by the specific target molecule. Along with converting riboswitches from simple ON to OFF state and vice-versa, a change in the each state to respond at ligand concentrations higher or lower than the half-maximal effective concentration (EC_{50}) of the natural or originally constructed ones are often desired for biomedical and biotechnological applications such as 1) synthesis of metabolites in microorganisms to levels higher than the natural intracellular concentration;[4] 2) balanced regulation of expression from multiple genes for production of recombinant proteins[5] or natural products;[6] and 3) reduction of the EC_{50} concentration of drug to overcome drug resistance. Currently, it is very difficult to rationally tune the EC_{50}s of aptamers, and new approaches are needed to enable design of controllable riboswitch aptamer domains.

As an alternative to traditional in vitro aptamer selection,[7] aptamers have been produced by reengineering pre-existing aptamer domains derived from natural riboswitches.[8] This approach is promising; however, only a few riboswitch aptamers have been successfully reengineered to date.[8] Since riboswitch-mediated control of gene expression relies on binding kinetics and affinity of the ligand for the aptamer domain,[3] it is important to identify interior "tuning" regions of the aptamers responsible for these ligand binding parameters. If the tuning mechanism were understood, ligand-dependent gene expression could be artificially altered by rational design of the tuning regions of the riboswitches.

We envisaged that comparative analysis of kinetic parameters of the riboswitch aptamers that bind to the same ligand would provide insight into relationship between the aptamer sequence and its ligand binding properties. This is possible because different bacterial species employ the same class of riboswitch aptamers to regulate genes with different control mechanisms.[3] Here, we studied aptamer domains derived from flavin mononucleotide (FMN) riboswitches to identify variable tuning regions that can be altered to modulate FMN binding kinetics and affinity. FMN riboswitches are involved in the biosynthesis and transport of riboflavin (vitamin B2). Riboflavin is a direct precursor of the flavin nucleotides, FMN and flavin adenine dinucleotide (FAD), which mediate essential oxidation–reduction reactions when bound to flavoproteins.[4] We chose the FMN riboswitch for the present study owing to its therapeutic[9] and biotechnological[10] relevance.

Previous sequence alignment[11] and X-ray crystallography[12] studies demonstrated a unique structure of FMN riboswitch aptamers consists of six stems (P1–P6) and five loops (L2–L6) (Figure 1 a,b; Supporting Information, Figure S1). The evolutionary conservation of stem orientations and their variable base-pair compositions in FMN aptamers[11] suggested to us that the stem regions tune the riboswitch responsiveness to FMN in each organism. Here, we focused on Watson–Crick (G·C and A·T) and non-Watson–Crick (G·U) base-pairs and their sequence context in stems P3, P4,

[*] Dr. A. B. Rode, Dr. T. Endoh, Prof. Dr. N. Sugimoto
Frontier Institute for Biomolecular Engineering Research (FIBER)
Konan University
7-1-20 Minatojima-minamimachi, Kobe 650-0047 (Japan)
E-mail: sugimoto@konan-u.ac.jp

[**] This work was supported in part by Grants-in-Aid for Scientific Research and MEXT (Japan)-Supported Program for the Strategic Research Foundation at Private Universities, the Hirao Taro Foundation of the Konan University Association for Academic Research, and the Chubei Itoh Foundation.

Supporting information for this article is available on the WWW under http://dx.doi.org/10.1002/anie.201407385.

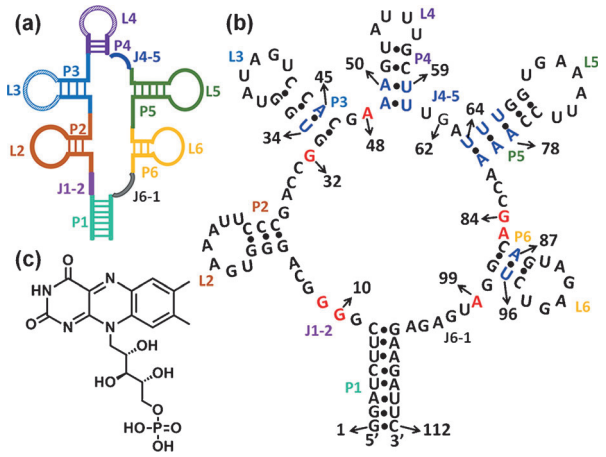

Figure 1. a) The conserved secondary structure of FMN aptamer. Stem (P1–P6), loop (L2–L6), and junction (J1-2, J4-5, and J6-1) regions are depicted in different colors. Two additional non-conserved stem-loops on the top of loops L3 and L4 are indicated with dashed lines. b) Secondary structure of *F. nucleatum* riboswitch aptamer sequence (aptamer **1**). The position of the nucleotide from the 5′ end of aptamer is indicated by the number next to arrow. The nucleotides in red are involved in the interaction with FMN and the base-pairs positions mutated in this study are shown in blue. c) Chemical structure of FMN.

P5, and P6. To assess whether these base-pair variations affect FMN binding properties, we investigated ligand binding kinetics of several FMN riboswitch aptamers. We selected FMN riboswitch aptamers **1** to **8** with different lengths and sequence compositions (Supporting Information, Table S1, entries 1–8).[11b] Each riboswitch aptamer was selected from a different bacterial genome, and thus there is significant sequence variation in the stem regions. Aptamer **1**, which is derived from riboflavin transporter *impX* gene of *F. nucleatum*, was chosen as its crystal structure has been solved.[12a] All of the aptamers were synthesized from DNA templates by in vitro transcription using T7 RNA polymerase as described in Supporting Information.

The binding kinetics of all selected riboswitch aptamers were quantitatively evaluated using stopped-flow fluorescence spectroscopy at 25 °C. Stopped-flow fluorescence spectroscopy has been used to monitor kinetics of ligand binding and aptamer folding in various riboswitch classes including the FMN riboswitches.[3a] To study binding kinetics, we made use of intrinsic fluorescent properties of FMN (Figure 1 c). The fluorescence intensity of FMN decreases with a change in RNA aptamer conformation.[3a] A decrease in fluorescence intensity of FMN was observed after addition of each of the aptamers **1** to **8** indicating that all the selected riboswitch aptamers have ability to bind FMN (data not shown). The kinetic data obtained at different concentrations of aptamer were fitted by a pseudo first-order equation S1 to obtain apparent rate constant k_{app} (Supporting Information, Figure S2 a). The association rates k_a and dissociation rates k_d of the FMN binding to the riboswitch aptamers were calculated by plotting k_{app} versus RNA concentration (Supporting Information, Figure S2 b and Equation (S2)). The equilibrium dissociation constant (K_D) was calculated from k_a and k_d values.

Table 1 shows k_a, k_d, and K_D values for FMN binding to aptamers **1** to **8**. The data are arranged in decreasing order of k_d values. Aptamer **7** (with one U·A base pair in stem P5) and aptamer **2** (with four U·A pairs and one U·G base pair) bound FMN with highest ($3.02\times10^5\,L\,mol^{-1}\,s^{-1}$) and lowest ($0.68\times10^5\,L\,mol^{-1}\,s^{-1}$) association rate constants, respectively. Aptamer **1** (with seven non-G·C pairs) and aptamer **8** (with all G·C base pairs) had the highest ($37.9\times10^{-3}\,s^{-1}$) and the lowest ($0.72\times10^{-3}\,s^{-1}$) dissociation rate constants, respectively. The k_a and k_d parameters reported here are in the range of previously reported kinetic parameters for other natural FMN aptamers.[3a] The K_D values ranged from 321 nM to 3.2 nM (a 100-fold difference).

Table 1: Kinetic parameters of FMN binding with selected natural aptamers.[a]

Aptamer	Bacteria name		Stem no. with base-pair compositions				Kinetic parameters		
no.	abbreviation[b]		P3	P4	P5	P6	k_a [10^5 L mol^{-1} s^{-1}]	k_d [10^{-3} s^{-1}]	K_D [10^{-8} mol L^{-1}]
1	(FN)	3′	C **A** C C	**U U**	**A A A** C C	G **U** C	1.50 ± 0.14	37.9 ± 1.35	25.2
		5′	G **U** G G	**A A**	**U U U** G G	C **A** G			
2	(DF)	3′	C G C C	**U** G	**A A A** C C	G **U** C	0.68 ± 0.03	22.0 ± 1.12	32.1
		5′	G C G G	**G** C	**U U U** G G	C **A** G			
3	(BA)	3′	**U** G C C	G G	**G** G **A U** C	G **U** C	1.04 ± 0.03	12.8 ± 0.64	12.2
		5′	**G** C G G	C C	**U** C **U A** G	C **A** G			
4	(BH)	3′	**U** G C C	G G	G G **G** C C	G **U** C	0.80 ± 0.06	8.24 ± 1.01	10.7
		5′	**G** C G G	C C	C C **U** G G	C **A** G			
5	(VK)	3′	C **A** C C	C G	**A A A** C C	G **U** C	1.28 ± 0.04	6.87 ± 0.88	5.35
		5′	G **U** G G	G C	**U U U** G G	C **A** G			
6	(DHA)	3′	C G C C	**A** G	G **A A** C C	G C C	0.77 ± 0.00	3.42 ± 0.18	4.45
		5′	G C G G	**U** C	C **U U** G G	C G G			
7	(BP)	3′	C G C C	C G	G G **A** C C	G C C	3.02 ± 0.04	1.67 ± 0.47	0.55
		5′	G C G G	G C	C C **U** G G	C G G			
8	(PU)	3′	C G C C	C G	G G G C C	G C C	2.25 ± 0.04	0.72 ± 0.27	0.32
		5′	G C G G	G C	C C C G G	C G G			

[a] The nucleotides in bold indicate non-G·C base-pair compositions in selected aptamer helices; in P3 and P4 only highly conserved base pairs near binding pocket are shown. [b] Full names of bacterial species and complete sequences are given in the Supporting Information.

The variations in K_D values (with the exception of aptamer **2**) are due to differences in k_d (52.6-fold difference) rather than differences in k_a (4.44-fold difference). The aptamers with the same numbers of non-G·C base pairs (five in aptamers **2**, **3**, and **5** and three in aptamers **4** and **6**) had different dissociation rate constants that depended on sequence context of the non-G·C pairs. Aptamer **7** with one A·U base pair in the centre of P5 had a dissociation rate constant 2.32-fold higher than that of aptamer **8** with all G·C base pairs. These results suggest that the non-G·C base pair composition has an effect on the dissociation rate constant. However, not only the number of the non-G·C base pairs but also their locations and sequence contexts affect the kinetic parameters.

The observed differences in GC contents at the stem region and kinetic parameters among studied aptamers might be result of variation in habitat temperature of bacteria from which they are derived. However, the bacteria from which these natural aptamers are derived grow optimally at 37 °C with the exceptions of *Bacillus halodurans* (aptamer **4**) and *Pseudomonas fluorescens* (aptamer **8**), which grow optimally at 30 °C. Thus, there is no correlation between optimal growth temperatures and kinetic parameters. Another possible explanation for observed kinetic differences is that these aptamers control operons/genes that encode different proteins required for riboflavin synthesis/transport.[11b] Kinetic and affinity variations may ensure appropriate synthesis of the riboflavin in each bacterium as riboflavin requirements differ.

Table 1 shows relationship between base-pair compositions in stem regions and k_a, k_d, and K_D values; however, the riboswitch aptamers have sequence variations in non-conserved single-stranded regions (loops and junctions) as well. The variations in the single-stranded regions might result in the differences of the kinetic parameters. The sequence alignment and secondary structures of the riboswitch aptamers predicted by mfold[13] are shown in the Supporting Information, Table S1 and Figures S3–S10, respectively. To determine the sequence basis for observed kinetic parameter differences, we systematically mutated the non-G·C base pairs in P3, P4, P5, and P6 regions of aptamer **1**[12a] to compensatory G·C base pairs. All mutated aptamer sequences and their predicted secondary structures are shown in the Supporting Information, Table S1, entries 9–16, and in Figures S11–S18. We made five types of mutants that replaced A·U with G·C pairs: 1) Replacements of single base pairs in each of P3, P4, P5, and P6 stems (aptamers **9**–**12**); 2) replacements of closing base pairs in P4 and P5 (aptamer **13**); 3) replacements of three consecutive A·U base pairs in P5 (aptamer **14**); 4) replacement of all seven A·U base pairs (aptamer **15**); and 5) replacement of all seven A·U base pairs along with replacement of U61, which may pair with A48 (Figure 1 b), with A61 (aptamer **16**). Mutations were designed to create a G·C base pair in the same orientation as that of the G·C base pair at the equivalent position in aptamer **8**, which showed highest affinity among the originally tested riboswitch aptamers (aptamers **1**–**8**). On a native gel run in buffer containing cations in the same concentrations as used in the stopped-flow experiment, the mutant aptamers (aptamers **9** to **16**) migrated to the same extent as aptamer **1** (Supporting Information, Figure S19). This suggests that folding of these mutants was similar to that of the wild type.

The k_a, k_d, and K_D values of the mutated aptamers **9** to **16** were obtained by the stopped-flow fluorescence spectroscopy at 25 °C (Table 2). All of the mutations decreased k_d and K_D compared to wild-type aptamer **1**. The observed difference in k_d was larger (11.5-fold) than that of k_a values (2.46-fold). K_D values of wild-type and mutant aptamers ranged from 252 nM to 21.7 nM. The observed differences in apparent rate constants between aptamer **1**, which had the lowest affinity, and mutated aptamer **16**, with highest affinity, are shown in the Supporting Information, Figure S20. The single base-pair mutations in different stems had different influences on kinetic parameters. In the case of the single base-pair mutations inside stems, aptamer **12** had a higher binding affinity than aptamer **9** owing to a lower k_d value. In contrast, for mutations at the closing positions of a stem (aptamers **10** and **11**), the difference in the binding affinities was mainly due to a difference in k_a value. The combination of mutations at two closing base pairs in aptamer **13** showed an adverse synergistic effect on k_d and K_D compared to aptamers with these individual mutations (aptamers **10** and **11**). As we observed extensive variation of base pairs in P5, we mutated three A·U base-pairs of only P5 (aptamer **14**). The parameters for aptamer **14** had no clear relationship to parameters of aptamers with one (aptamer **11**) or combined mutations (aptamer **13**). The mutated aptamer with highest G·C composition showed lowest dissociation rate constant and highest affinity (aptamers **15** and **16**). These results suggest that both stem base pair composition and the sequence context influence ligand binding parameters. This finding supports our recent[14] and other group's[15] observations that demonstrated importance of stem regions in another class of aptamer on ligand binding affinity. We mutated U61 in aptamer **15** to obtain aptamer **16**. This position is not highly conserved; only aptamer **2** also has a U at this position. This mutation may disturb intercalation of FMN between A48 and A85 (Supporting Information, Figure S21)[12a] by forming an A·U base pair with A48. We observed an increase in k_a and decreases in k_d and K_D values for aptamer **16** in comparison with aptamer **15**.

Along with the above mutants of aptamer **1**, we constructed aptamer **17** (Supporting Information, Figure S22), in which seven G·C base pairs in aptamer **8** were mutated to A·U base pairs, to confirm whether the less stable tuning region based on A·U base pairs inversely decrease the affinity. The aptamer **17** showed 200-fold increase in K_D values (641 nM) compared to its wild type aptamer **8** (3.2 nM) (Supporting Information, Figure S22). These results suggest the importance of base pairs identities in controlling ligand binding properties.

Based on previous studies of ligand binding with RNA aptamers, it was suggested that the FMN aptamer adopts a pre-folded state in the absence of FMN, and only a small structural transition occurs within the junction region of the binding pocket during FMN binding.[12a] If this is the case, diffusion of FMN will be the rate-limiting step in association of the ligand.[3] The comparatively small range (4.44-fold) in

Table 2: Kinetic parameters of FMN binding to mutants of aptamer **1**.[a]

Aptamer no.	Mutated base pair position[b]	Stem and junction regions with nucleotide compositions																				Kinetic parameters		
		P3				P4			J4-5			P5					P6						k_a [10^5 L mol^{-1} s^{-1}]	k_d [10^{-3} s^{-1}]	K_D [10^{-8} mol L^{-1}]
		3′–46	45	44	43	60	59					80	79	78	77	76	97	96	95					
9	P3_m34	C	**G**	C	C	U	U	U	G	A		A	A	A	C	C	G	U	C			1.14 ± 0.02	19.9 ± 1.04	17.5
		G	**C**	G	G	A	A					U	U	U	G	G	C	A	G					
		5′–33	34	35	36	49	50	61	62	63		64	65	66	67	68	86	87	88					
10	P4_m49	C	A	C	C	**C**	U	U	G	A		A	A	A	C	C	G	U	C			2.73 ± 0.18	29.9 ± 0.76	11.0
		G	U	G	G	**G**	A					U	U	U	G	G	C	A	G					
11	P5_m64	C	A	C	C	U	U	U	G	A		**G**	A	A	C	C	G	U	C			1.65 ± 0.10	24.1 ± 1.29	14.7
		G	U	G	G	A	A					**C**	U	U	G	G	C	A	G					
12	P6_m87	C	A	C	C	U	U	U	G	A		A	A	A	C	C	G	**C**	C			1.14 ± 0.03	14.3 ± 0.96	12.6
		G	U	G	G	A	A					U	U	U	G	G	C	**G**	G					
13	P4_m49 & P5_m64	C	A	C	C	**C**	U	U	G	A		**G**	A	A	C	C	G	U	C			1.70 ± 0.04	32.6 ± 0.95	19.2
		G	U	G	G	**G**	A					**C**	U	U	G	G	C	A	G					
14	P5_m64,65,66	C	A	C	C	U	U	U	G	A		**G**	**G**	**G**	C	C	G	U	C			2.00 ± 0.04	30.4 ± 0.74	15.2
		G	U	G	G	A	A					**C**	**C**	**C**	G	G	C	A	G					
15	PAll_mAll	C	**G**	C	C	**C**	**G**	U	G	A		**G**	**G**	**G**	C	C	G	**C**	C			1.11 ± 0.02	9.25 ± 0.61	8.31
		G	**C**	G	G	**G**	**C**					**C**	**C**	**C**	G	G	C	**G**	G					
16	PAll_mAll & J_m61[c]	C	**G**	C	C	**C**	**G**	**A**	G	A		**G**	**G**	**G**	C	C	G	**C**	C			1.52 ± 0.05	3.30 ± 0.27	2.17
		G	**C**	G	G	**G**	**C**					**C**	**C**	**C**	G	G	C	**G**	G					

[a] The base pairs and nucleotides in bold are positions of mutations. [b] P and J indicate helix or junction, respectively, as in Figure 1 a. Numbers in bold above and below the sequence of aptamer **9** indicate positions relative to the 5′ end of aptamer **1**. [c] Along with stem region mutations, U61 was mutated to A.

association rate constants among the eight natural riboswitch aptamers evaluated here support this hypothesis. In contrast, the FMN dissociation rate constant depends on the strength of various short-range interactions within its tertiary structure such as hydrogen bonding and stacking. Since the FMN is encapsulated within a butterfly-like structure formed by interactions among the helices,[12a] these helices may open partially or fully when FMN dissociates from the aptamer. The opening rates of the helices will be affected by the base-pair compositions and sequence context.[16] Thus, replacement of A·U or G·U pairs with a more stable G·C base pair should result in an increase in helical stability and a reduction of the FMN dissociation rate constant. This is indeed what we observed in our comparison of mutated aptamers compared to the wild type. These results suggest that the observed decrease in affinity values is mainly due to decrease in dissociation rates and not due to gross changes in native conformation or impairment of the direct interaction with ligand. Thus the compensatory base-pair mutation approach is advantageous to generate high affinity aptamers for biological applications, as it has ability to avoid non-specificity issue of the aptamer, which may result from large conformational changes.

To investigate whether the EC_{50} values of FMN-dependent gene regulation can be "tuned" by alteration in base pairs, we designed artificial riboswitches based on aptamer **1** (wild type), aptamer **16** (G·C mutated), and control aptamer, in which the nucleotides directly binding with FMN were mutated (Supporting Information, Figures S23–S25). In the artificial riboswitches, we designed stem-loop structures downstream of the FMN aptamer in such a way that the ribosome-binding site (RBS) will be exposed on a single-stranded region in the absence of FMN to turn gene expression ON. In the presence of FMN, the RBS will be sequestered in a stem-loop to block translation initiation and turn the gene expression OFF (Supporting Information, Figure S26). The artificial riboswitch sequences were inserted between T7 promoter and *Renilla luciferase* coding sequences. Assays were performed using an in vitro coupled transcription/translation system. Gene expression levels were evaluated by measuring the luminescence signals from *Renilla* luciferase after a 30 min reaction at 37 °C (Figure 2).

The luminescence intensity decreased with increasing FMN concentration for the artificial riboswitches based on both aptamer **1** and aptamer **16**, while control riboswitch did not show any changes in gene expression. The magnitude of decrease was significantly different between the riboswitches

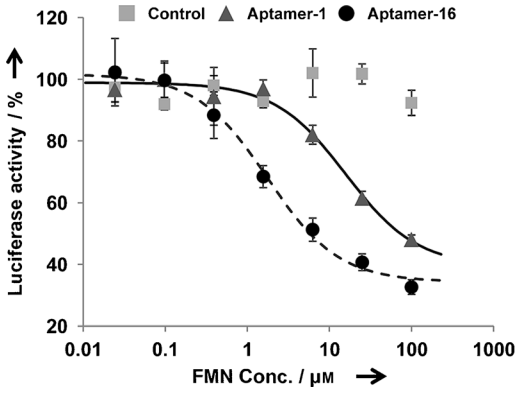

Figure 2. In vitro coupled transcription/translation of artificial riboswitches consists of aptamers **1**, **16**, and control. In vitro experiments were performed for each riboswitch over a range of concentrations of FMN (24.4 nM to 100 μM). The luciferase activity at 0 nM FMN concentration was defined as 100%. Each data point is the average of four independent experiments. Fitting curves for aptamer **1** and aptamer **16** are shown with solid and dashed lines, respectively.

based on aptamers **1** and **16**. EC_{50} values were estimated by fitting the plot of the relative luciferase activity versus FMN concentration (Supporting Information, equation (S3)). The EC_{50} values for the artificial riboswitches based on aptamer **1** and **16** were 16.3 ± 3.45 and 1.76 ± 0.17 μM, respectively. The compensatory A·U to G·C mutation increased FMN sensitivity in the aptamer **16**-based artificial riboswitch comparing to that of the aptamer **1**-based system resulting in a 9.31-fold reduction in the EC_{50} value that corresponded to the 11.6-fold differences in K_D values between parental aptamer **1** and aptamer **16**. These results suggest that the gene expression can be tuned by rationally controlling ligand binding properties by adjusting compensatory base pairs in the tuning regions.

In summary, the dissociation rate constant and affinity of the RNA aptamer for FMN depends on base-pair composition and sequence context in the aptamer helices. Aptamers with higher G·C base-pair compositions have smaller differences in k_a, but significantly lower k_d and K_D values relative to those with more A·U and G·U pairs. The observed large differences in dissociation rate (52.6-fold) and affinity (100-fold) among natural aptamer domains suggested that the compensatory base-pair variations in the natural riboswitch aptamers might ensure appropriate levels of synthesis of riboflavin in each bacterium. Furthermore, we performed tuning of FMN-dependent gene regulation in vitro by rational design of artificial riboswitches based on the kinetic results. The FMN-dependent riboswitch control prevents accumulation of large amounts of FMN and FAD, which are important materials in pharmaceutical and food industries, because expression of flavin nucleotides synthesis genes depends on the EC_{50} value of the riboswitch.[4] Tuning of the EC_{50} value by selecting appropriate A·U and G·U base-pair compositions in variable stem regions as demonstrated here would be helpful for various industrial applications such as cost-effective production of flavin nucleotides in bacteria. The tuned aptamers may also be utilized for construction of artificial riboswitches for controlling expression of genes other than those involved in riboflavin synthesis.

Received: July 19, 2014
Revised: September 17, 2014
Published online: December 2, 2014

Keywords: aptamers · flavin mononucleotides · gene regulation · kinetics · riboswitches

[1] a) P. Ketzer, J. K. Kaufmann, S. Engelhardt, S. Bossow, C. V. Kalle, J. S. Hartig, G. Ungerechts, D. M. Nettelbeck, *Proc. Natl. Acad. Sci. USA* **2014**, *111*, E554 – E562; for more reference see Supporting Information.

[2] a) A. Ogawa, *RNA* **2011**, *17*, 478 – 488; b) M. Wieland, A. Benz, B. Klauser, J. S. Hartig, *Angew. Chem. Int. Ed.* **2009**, *48*, 2715 – 2718; *Angew. Chem.* **2009**, *121*, 2753 – 2756; c) M. Wieland, J. S. Hartiq, *Angew. Chem. Int. Ed.* **2008**, *47*, 2604 – 2607; *Angew. Chem.* **2008**, *120*, 2643 – 2646.

[3] a) J. K. Wickiser, W. C. Winkler, R. R. Breaker, D. M. Crothers, *Mol. Cell* **2005**, *18*, 49 – 60; b) J. K. Wickiser, M. T. Cheah, R. R. Breaker, D. M. Crothers, *Biochemistry* **2005**, *44*, 13404 – 13414; for more references, see the Supporting Information.

[4] C. A. Abbas, A. A. Sibirny, *Microbiol. Mol. Biol. Rev.* **2011**, *75*, 321 – 360.

[5] C. Bieniossek, Y. Nie, D. Frey, N. Olieric, C. Schaffitzel, I. Collinson, C. Romier, P. Berger, T. J. Richmond, M. O. Steinmetz, I. Berger, *Nat. Methods* **2009**, *6*, 447 – 450.

[6] B. F. Pfleger, D. J. Pitera, C. D. Smolke, J. D. Keasling, *Nat. Biotechnol.* **2006**, *24*, 1027 – 1032.

[7] a) C. Tuerk, L. Gold, *Science* **1990**, *249*, 505 – 510; b) A. D. Ellington, J. W. Szostak, *Nature* **1990**, *346*, 818 – 822.

[8] a) N. Dixon, J. N. Duncan, T. Geerlings, M. S. Dunstan, J. E. G. McCarthy, D. Leys, J. Micklefield, *Proc. Natl. Acad. Sci. USA* **2010**, *107*, 2830 – 2835; b) N. Dixon, C. J. Robinson, T. Geerlings, J. N. Duncan, S. P. Drummond, J. Micklefield, *Angew. Chem. Int. Ed.* **2012**, *51*, 3620 – 3624; *Angew. Chem.* **2012**, *124*, 3680 – 3684.

[9] a) K. F. Blount, R. R. Breaker, *Nat. Biotechnol.* **2006**, *24*, 1558 – 1564; b) J. E. Barrick, R. R. Breaker, *Genome Biol.* **2007**, *8*, R239.

[10] a) C. M. Burgess, E. J. Smid, G. Rutten, D. V. Sinderen, *Microb. Cell Fact.* **2006**, *5*, 24.

[11] a) M. S. Gelfand, A. A. Mironov, J. Jomantas, Y. I. Kozlov, D. A. Perumov, *Trends Genet.* **1999**, *15*, 439 – 442; b) A. G. Vitreschak, D. A. Rodionov, A. A. Mironov, M. S. Gelfand, *Nucleic Acids Res.* **2002**, *30*, 3141 – 3151.

[12] a) A. Serganov, L. Huang, D. J. Patel, *Nature* **2009**, *458*, 233 – 237; b) Q. Vicens, E. Mondragon, R. T. Batey, *Nucleic Acids Res.* **2011**, *39*, 8586 – 8598.

[13] M. Zuker, *Nucleic Acids Res.* **2003**, *31*, 3406 – 3415.

[14] V. Kumar, T. Endoh, K. Murakami, N. Sugimoto, *Chem. Commun.* **2012**, *48*, 9684 – 9686.

[15] a) A. Reining, S. Nozinovic, K. Schlepckow, F. Buhr, B. Furtig, H. Schwalbe, *Nature* **2013**, *499*, 355 – 359; b) C. D. Stoddard, J. Widmann, J. J. Trausch, J. G. Marcano-Velazquez, R. Knight, R. T. Batey, *J. Mol. Biol.* **2013**, *425*, 1596 – 1611.

[16] P. L. Vanegas, T. S. Horwitz, B. M. Znosko, *Biochemistry* **2012**, *51*, 2192 – 2198 and references therein.

